THE ASTROPHYSICAL JOURNAL, 525:799–807, 1999 November 10
© 1999. The American Astronomical Society. All rights reserved. Printed in U.S.A.

A MODEL FOR THE SCATTERED LIGHT CONTRIBUTION AND POLARIZATION OF THE DIFFUSE Hα GALACTIC BACKGROUND

KENNETH WOOD[1] AND R. J. REYNOLDS[2]
Received 1999 March 23; accepted 1999 June 23

ABSTRACT

We present Monte Carlo simulations of the diffuse Hα Galactic background. Our models comprise direct and multiply scattered Hα radiation from the kpc scale height warm ionized medium and midplane H II regions. The scattering is off dust that is assumed to be well mixed with the gas, with an axisymmetric density distribution taken from the literature. The results of our simulations are all-sky Hα images that enable us to separate out the contributions of direct and scattered radiation. We also determine how far the model Hα photons have traveled, i.e., how far we see into the Galaxy at Hα. Our models reproduce the overall characteristics of the observed Hα background and predict that the scattered Hα intensity at high latitudes is in the range 5%–20% of the total intensity, in agreement with estimates based on [S II]/Hα and [O III]/Hα line ratio measurements. The polarization arising from dust scattering of Hα from midplane H II regions is predicted to be less than 1% at high latitude.

Subject headings: diffuse radiation — dust, extinction — H II regions — polarization — radiative transfer

1. INTRODUCTION

Ubiquitous but faint Hα proves the presence of the warm ionized medium (WIM), a major but poorly understood component of the interstellar medium (ISM) containing the majority of the ionized gas in the Galaxy (see a review by Reynolds et al. 1995). The ionized gas is seen at all Galactic latitudes and has a scale height of about 900 pc (judged from the dispersion measure of the radio signals from pulsars in globular clusters), a temperature of around 10,000 K, and volume-filling factor in the range 0.1–0.4. In the solar neighborhood, the total power represented by the ionizations producing the Hα is about 15% of the total ionizing rate from OB stars, or about 100% of the power ejected by supernovae. The source of ionization is not well understood and has been narrowed down to either (*a*) the leakage of the ionizing photons from OB stars to the diffuse ionized gas, which actually provides the correct spectrum of the O, N, and S ions (Domgörgen & Mathis 1994; see also Dove & Shull 1994; Dove, Shull, & Ferrara 1999; Miller & Cox 1993; Elmegreen 1998), or (*b*) some unknown, more distributed source of ionization (Sciama 1995).

Low spatial resolution mapping of the Hα emission (Reynolds 1990) has revealed the following characteristics:

1. At low latitudes ($|b| < 10°$) the Galactic midplane is dominated by Hα emission from bright H II regions.
2. At intermediate Galactic latitudes ($10° < |b| < 50°$) the Hα intensity follows a csc $|b|$ law with the average intensity being $\langle I_\alpha \sin |b| \rangle \approx 1R$, where $R = 10^6/4\pi$ Hα photons s^{-1} cm^{-2} sr^{-1}.
3. Above $|b| = 50°$ the emissivity appears to be about a factor of 2 below the csc $|b|$ law for lower latitudes.
4. Localized departures from the csc $|b|$ law are evident at all latitudes, indicating the clumpy and filamentary nature of the WIM. These features are becoming more evident through early results from the Wisconsin Hα Mapper (WHAM) all-sky survey (Reynolds et al. 1998; Haffner, Reynolds, & Tufte 1998).

The Galactic contributions to the Hα background are direct and scattered Hα from the WIM, direct Hα from midplane H II regions, and Hα from H II regions that is scattered by dust at high latitudes. Observations of [S II]/Hα line ratios along sight lines at low latitude (toward midplane H II regions) and at high latitudes in the diffuse ISM (Reynolds 1988) show that the line ratios in the diffuse ISM are larger by up to a factor of 10 than those in traditional H II regions. This indicates that the ionization state of the WIM is very different from that of H II regions, and based on these observations, Reynolds (1990) concluded that the scattered component from midplane H II regions was at most 15% of the total Hα intensity.

Ferrara et al. (1996) presented a radiation transfer model for Hα emission and scattering in the edge-on galaxy NGC 891. They found that at 600 pc from the midplane, the scattered light from H II regions is around 10% of the total Hα intensity. Their models also predict a dust-scattered polarization of less than 1%. The analysis that we present in this paper is very similar to that of Ferrara et al. (1996), except that we are now viewing the radiation transfer simulation from inside the Galaxy. Our goal is to determine, from a theoretical/modeling perspective, the relative contributions of direct and scattered Hα at high latitudes, how large a region of the ISM contributes to the observed intensity, and whether our models can reproduce the general characteristics of the Hα background. In addition, we present a prediction of the polarization arising from dust scattering of the Hα emission. The ingredients of our models are presented in § 2, and the scattered light models and polarization predictions are presented in §§ 3 and 4.

2. MODELS

We perform the radiation transfer with a three-dimensional Monte Carlo scattering code. We have previously modeled the polarization patterns and diffuse

[1] Smithsonian Astrophysical Observatory, 60 Garden Street, Cambridge, MA 02138; kenny@claymore.harvard.edu
[2] Astronomy Department, University of Wisconsin, 475 North Charter Street, Madison, WI 53703; reynolds@astro.wisc.edu

scattered light in external galaxies (Wood 1997; Wood & Jones 1997). These investigations adopted smooth axisymmetric models for the dust and illuminating starlight. In order to determine the propagation of starlight in clumpy media and simulate all-sky maps viewed from within a model galaxy, we have modified our codes to include the effects of scattering, clumping, dust scale heights, and source distributions in a three-dimensional Galactic model. The ingredients of our models are the Hα emissivity, dust density distribution and scattering parameters, and radiation transfer algorithm, described below.

2.1. *Density Grid*

Our model Galaxy density is constructed on a three-dimensional linear Cartesian grid comprising $201 \times 201 \times 201$ grid cells. The physical extent of our model galaxy is ± 15 kpc, so each grid cell is a cube of ≈ 150 pc on a side.

The number densities (cm^{-3}) for the five phases of the ISM (molecular, cold neutral, warm neutral, warm ionized, and hot ionized) are determined from analytic expressions presented by Ferrière (1998, eqs. [1]–[9]). This is a smooth axisymmetric model of the ISM. In the model at the solar radius the WIM has a scale height of 1 kpc and midplane number density of 0.0237 cm^{-3}. The neutral hydrogen is composed of three components: Gaussian scale heights of 127 and 318 pc and an exponential scale height of 403 pc with the total midplane number density (cold neutral plus warm neutral) being 0.566 cm^{-3}. We have also included the spiral arm density determined by Taylor & Cordes (1993). The spiral arms were inserted in our density grid using the FORTRAN subroutines that are described in the Appendix of Taylor & Cordes (1993). To complete our model ISM density we have inserted an evacuated region of 200 pc radius centered on the Sun's location. This approximately represents the low-density "Local Bubble" (e.g., Cox & Reynolds 1987), within the constraints of the grid size.

We assume that the dust and gas are well mixed in all phases of the ISM and that the dust-to-gas ratio is constant throughout the Galaxy. We have not attempted to model any vertical or horizontal dependence of the dust-to-gas ratio within the Galaxy as was speculated by Ferrara et al. (1996). This would involve a detailed modeling of many data sets including *IRAS*, Hα, and H I and is beyond the scope of our current investigation to estimate scattered light levels. The dust-scattering parameters are taken to be those of a standard ISM mixture (see § 2.3).

2.2. Hα *Emissivity*

The Hα emissivity comprises emission from the WIM and from H II regions. The WIM Hα emissivity is proportional to the square of the WIM density (eq. [7] in Ferrière 1998). In the neighborhood of the Sun and near the Galactic midplane, the mean density in the WIM is 0.025 cm^{-3} and the emissivity is 6.7×10^{-16} Hα photons $\mathrm{cm}^{-3}\ \mathrm{s}^{-1}$ (as derived in Reynolds 1990). Extrapolating this emissivity using the Ferrière density results in a total WIM emissivity from our model Galaxy of 10^{52} Hα photons s^{-1}.

Bright H II regions are the dominant source of Hα near the Galactic equator, with angular sizes ranging from arcminutes to tens of degrees. In order to approximate the amount and distribution of Hα from local H II regions, we have utilized the Garmany, Conti, & Chiosi (1982) catalog of O stars within 2.5 kpc of the Sun. This catalog provides the spectral type of the sources, and we convert this to a number of ionizing photons from each source using Table 1 of Miller & Cox (1993). We assume that 6% of the ionizing photons from each source escape the Galaxy (Bland-Hawthorn & Maloney 1999) and 15% go into producing the WIM (Reynolds 1990). Our escape fraction is consistent with the values of 6% and 3% (depending on star formation history) estimated from models by Dove, Shull, & Ferrara (1999). The remaining 79% from each source is assumed to produce local "point-source" H II regions with the Hα photon luminosity equal to $0.46 \times 0.79 N_{\mathrm{ionizing}} = 0.36 N_{\mathrm{ionizing}}$, assuming case B recombination (Martin 1988). We have assumed that $N_{\mathrm{H}\alpha} = 0.36 N_{\mathrm{ionizing}}$ for each source irrespective of location. This is clearly a simplification, since the Hα luminosity will depend on the local density, which in turn determines what fraction of ionizing photons escape the Galaxy, what fraction contributes to producing the WIM, and what fraction is converted to Hα within the local H II region. This calculation is beyond the scope of our current investigation and we therefore globally adhere to the relative fractions we have quoted. The model by Miller & Cox (1993) attributed the WIM Hα emission to extended "Strömgren volumes" created by OB associations, and such a scenario would also include Hα emission from supershells that may have formed around OB associations. Note that in our model we have separated the Hα into two components: a smooth component representing the extended emission of Miller & Cox and the point-source H II regions with Hα luminosities as described above.

For regions beyond 2.5 kpc (where the Garmany et al. catalog is incomplete) we extend the distribution of point sources by placing sources randomly in the molecular ring (from Ferrière 1998) and in the spiral arms (see Taylor & Cordes 1993). The (x, y) locations of all sources in our simulation are shown in Figure 1. We set the Hα luminosity of each of the additional randomly placed point sources at 10^{49} Hα photons s^{-1} (comparable to that of the Orion Nebula), and add enough sources so that the total luminosity of the H II regions in our simulation is equal to that of the WIM, $L_{\mathrm{H\,II}} = L_{\mathrm{WIM}} = 10^{52}$ Hα photons s^{-1}. Several authors have estimated the relative contributions of Hα from the WIM and H II regions in nearby spiral galaxies, with the ratio found to be in the range $0.47 < [\mathrm{H}\alpha(\mathrm{H\ II})/\mathrm{H}\alpha(\mathrm{TOTAL})] < 0.7$ for each galaxy as a whole (Ferguson, Wyse, & Gallagher 1996; Walterbos & Braun 1994; Veilleux, Cecile, & Bland-Hawthorn 1995). The relative Hα luminosities for the H II regions and the WIM in our simulation have been chosen to match this observational constraint.

2.3. *Opacity and Scattering Parameters*

We assume that the dust plus gas is represented by a Mathis, Rumpl, & Nordsieck (1977) mixture. The adopted parameters at Hα are a total opacity of 220 $\mathrm{cm}^2\ \mathrm{g}^{-1}$, albedo $a = 0.5$, and a scattering phase function given by the Henyey-Greenstein phase function, $\mathrm{HG}(\theta)$, with $g = 0.44$,

$$\mathrm{HG}(\theta) = \frac{1}{4\pi} \frac{1 - g^2}{(1 + g^2 - 2g \cos \theta)^{3/2}} . \quad (1)$$

The peak linear polarization, $p_l = 0.5$, is taken from White (1979). For the adopted densities and opacities, the total optical depth diametrically across the Galactic equator is $\tau_{\mathrm{eq}} \approx 50$, while at the Sun's radius, the total optical depth perpendicular to the Galactic disk is 0.4.

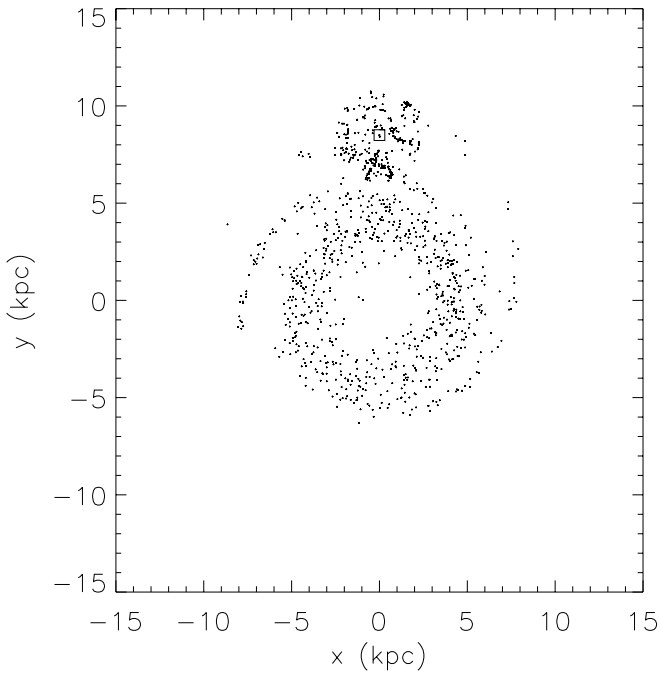

FIG. 1.—The x and y coordinates of the simulated point-source H II regions. Locations of O stars from the Garmany et al. (1982) catalog and random point sources distributed in the molecular ring (Ferrière 1998) and in the spiral arms (see Taylor & Cordes 1993). The Sun is located at (0, 8.5, 0).

There has been considerable interest in determining dust parameters in the diffuse ISM (Murthy & Henry 1995; Hurwitz 1994; Gordon et al. 1994), reflection nebulae (Calzetti et al. 1995), and protostellar clouds (Whitney, Kenyon, & Gomez 1997). The effects of changing the albedo and phase function asymmetry on scattered light patterns have been presented by other groups. Increasing or decreasing the albedo obviously increases or decreases the scattered light component. In their model of the UV diffuse Galactic light, Murthy & Henry (1995) showed that increasing g (making the phase function more forward-throwing) reduces the scattered light levels and concentrates the scattered light toward "halos" around the UV sources in their simulation. Bianchi, Ferrara, & Giovanardi (1996) also pointed out that the Henyey-Greenstein phase function may underestimate the forward scattering, and this would lead to a decrease in scattered light levels. Rather than repeat similar calculations for dust scattering of Hα, we note the effects of changing the albedo and phase function and keep the dust parameters fixed throughout our simulation.

2.4. *Radiation Transfer*

In our Monte Carlo radiation transfer we now use a scheme that includes "forced first scattering" and a "peeling-off" procedure as we force the photons toward the observer with the appropriate weights (see Appendix). We have adopted the forced first scattering in order to determine the scattered light contribution from scattering in optically thin, high-latitude regions. Our technique then determines the relative contributions of direct and multiply scattered Hα radiation from the WIM and H II regions.

One of the major questions in the study of the WIM is the source of its ionization. Current models (Miller & Cox 1993; Dove & Shull 1994; Dove et al. 1999; Elmegreen 1997) suggest that a clumpy ISM may allow photons to leak from the midplane H II regions to the high-latitude gas. While this paper is not investigating this problem, we are interested in determining how far the Hα probes into the Galaxy. To determine the distance that photons have traveled, we therefore construct three all-sky images. The first contains all photons, representing the total Hα intensity observed at Earth for this model. The two other images contain photons that originated from farther than 3 kpc and farther than 6 kpc; using the Monte Carlo technique, it is straightforward to "label" photons according to point of origin, distance traveled, number of scatterings, etc. Thus we can determine how far we "see" into the Galaxy model. We have also separated out direct and scattered Hα photons for the WIM and H II regions, thereby enabling us to quantify the role of dust scattering.

3. MODEL RESULTS

Figure 2 shows our all-sky simulation for the ISM model and illumination described above. The bright point sources have been scaled so that they are saturated at the maximum intensity from the direct WIM emission in the simulation. In Figure 3, 18° wide latitudinal cuts are shown for different Galactic longitudes. Each panel shows four curves: the heavy line is a csc $|b|$ law, and the three other curves show (*upper*) the total Hα intensity, (*middle*) scattered Hα from the point-source H II regions, and (*lower*) scattered Hα from the WIM. This simulation reproduces many of the observed features of the Galactic Hα emission. In particular, H II regions dominate at low latitudes, the csc $|b|$ law is closely followed at intermediate latitudes, and the intensity is lower than the csc $|b|$ law at high latitudes. These gross characteristics are all present in the data described by Reynolds (1990).

Departures from the csc $|b|$ law at high latitudes are seen not only in Hα but also in H I observations (Dickey & Lockman 1990). For H I, the fact that we are located in a local bubble is cited as the explanation for the departure. The Local Bubble is believed to be elongated perpendicular to the Galactic plane (Cox & Reynolds 1987; Snowden 1986), so there is a larger fraction of the H I column density "carved out" at high latitudes yielding the apparent departure from the csc $|b|$ law. The same effect will also be present at Hα, though at a smaller level because of the larger scale height of the WIM. However, in our simulations we approximated the Local Bubble as a sphere of radius 200 pc, yet we still found departures from the csc $|b|$ law at high latitudes. The reason for the departures in our simulations is the larger contribution of dust-scattered Hα at low latitudes. Figure 4 illustrates this by presenting a csc $|b|$ law and three curves comprising different components of the Hα intensity. The upper curve comprises the (direct plus scattered) WIM emission and the dust-scattered Hα from the point sources; the middle curve shows the (direct plus scattered) WIM Hα only; and the lower curve shows only the direct WIM emission. This figure clearly shows how scattered Hα is larger at low latitudes and yields the departures from the csc $|b|$ law at high latitudes. Note that for the direct WIM emission the csc $|b|$ law is closely followed at high latitudes, but dust obscuration is responsible for the emission being smaller than csc $|b|$ toward the midplane regions ($|b| < 10°$). In retrospect the departures are obvious, since the csc $|b|$ law is derived by integrating

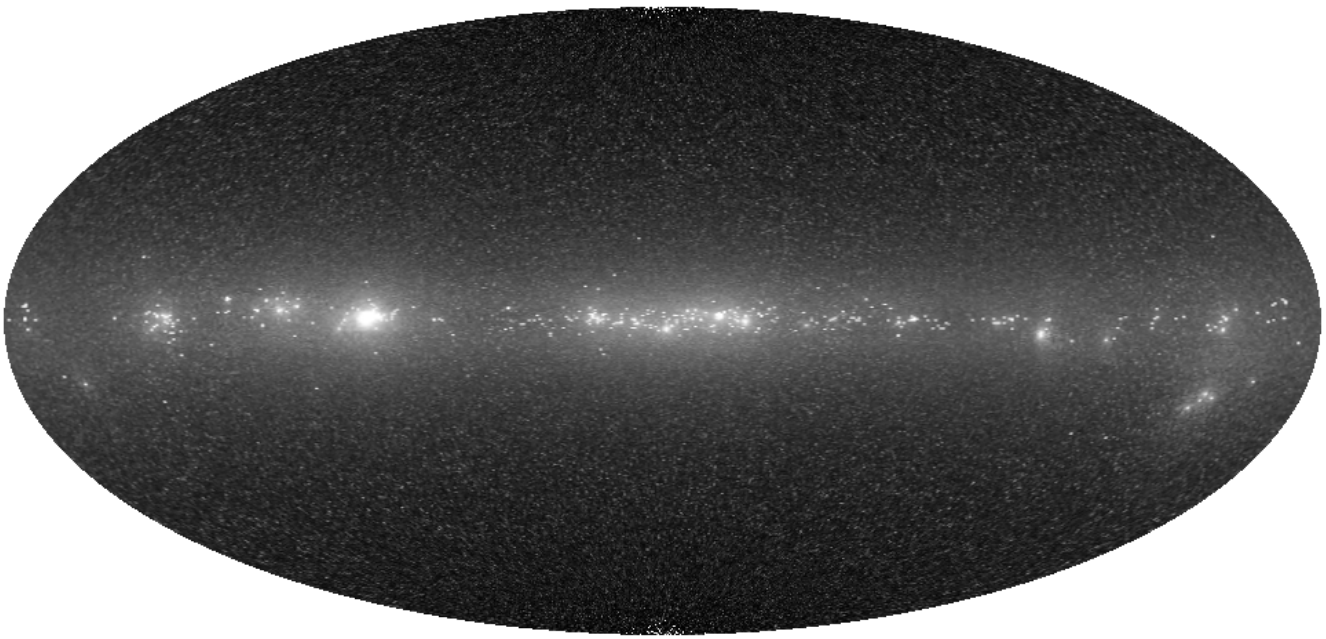

FIG. 2.—All-sky Aitoff projection of our Hα intensity simulation in Galactic coordinates (l, b). The Galactic center direction is at the center of the figure, and Orion is on the right below the midplane. The bright point sources have been saturated at the peak level of the direct WIM intensity, and the WIM and scattered light are shown on a square root stretch.

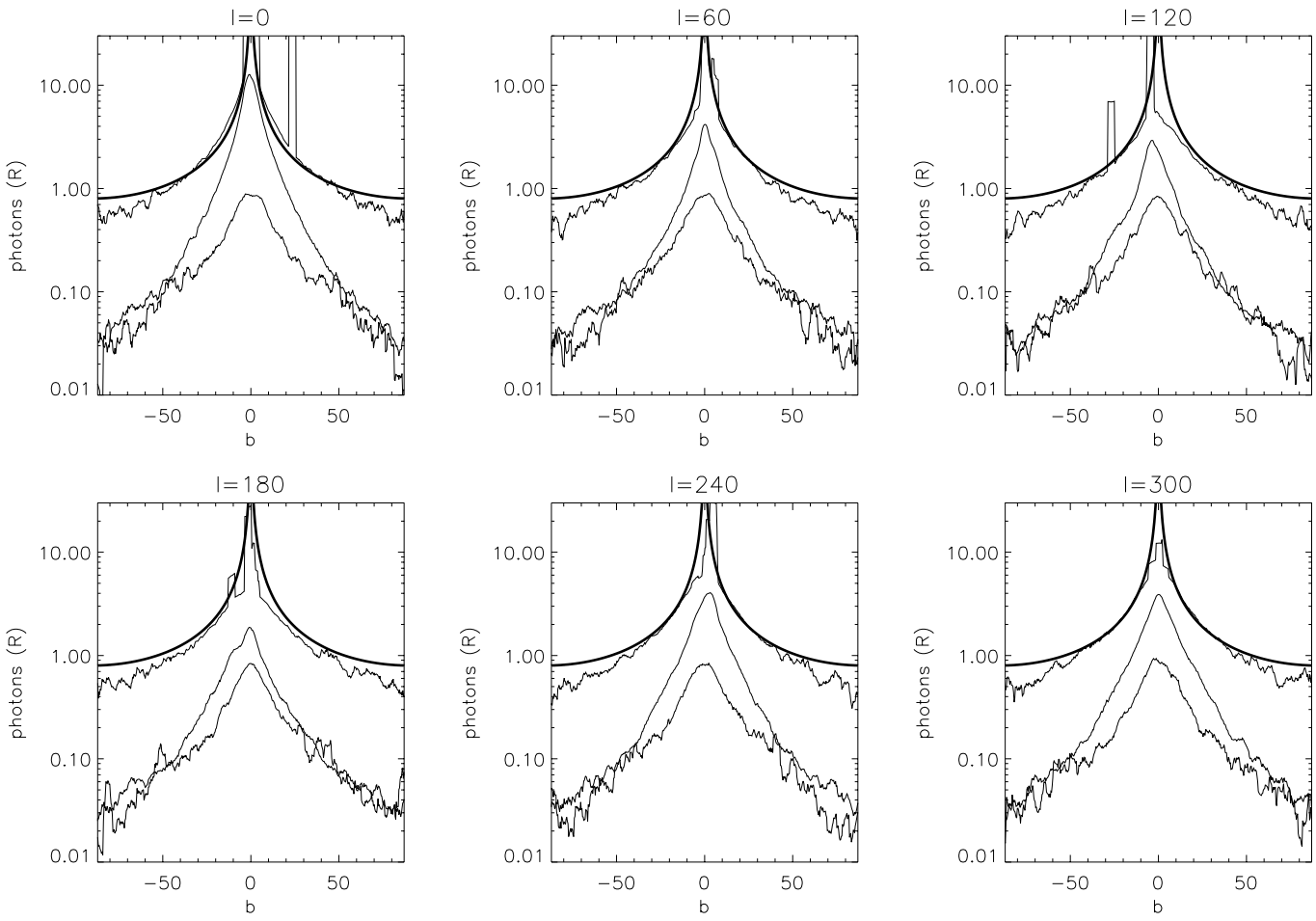

FIG. 3.—18° wide latitudinal intensity cuts through the simulation. The heavy curve shows a csc $|b|$ law; the three other curves show (*upper*) the total intensity, (*middle*) scattered light from point sources, and (*lower*) scattered light from the WIM.

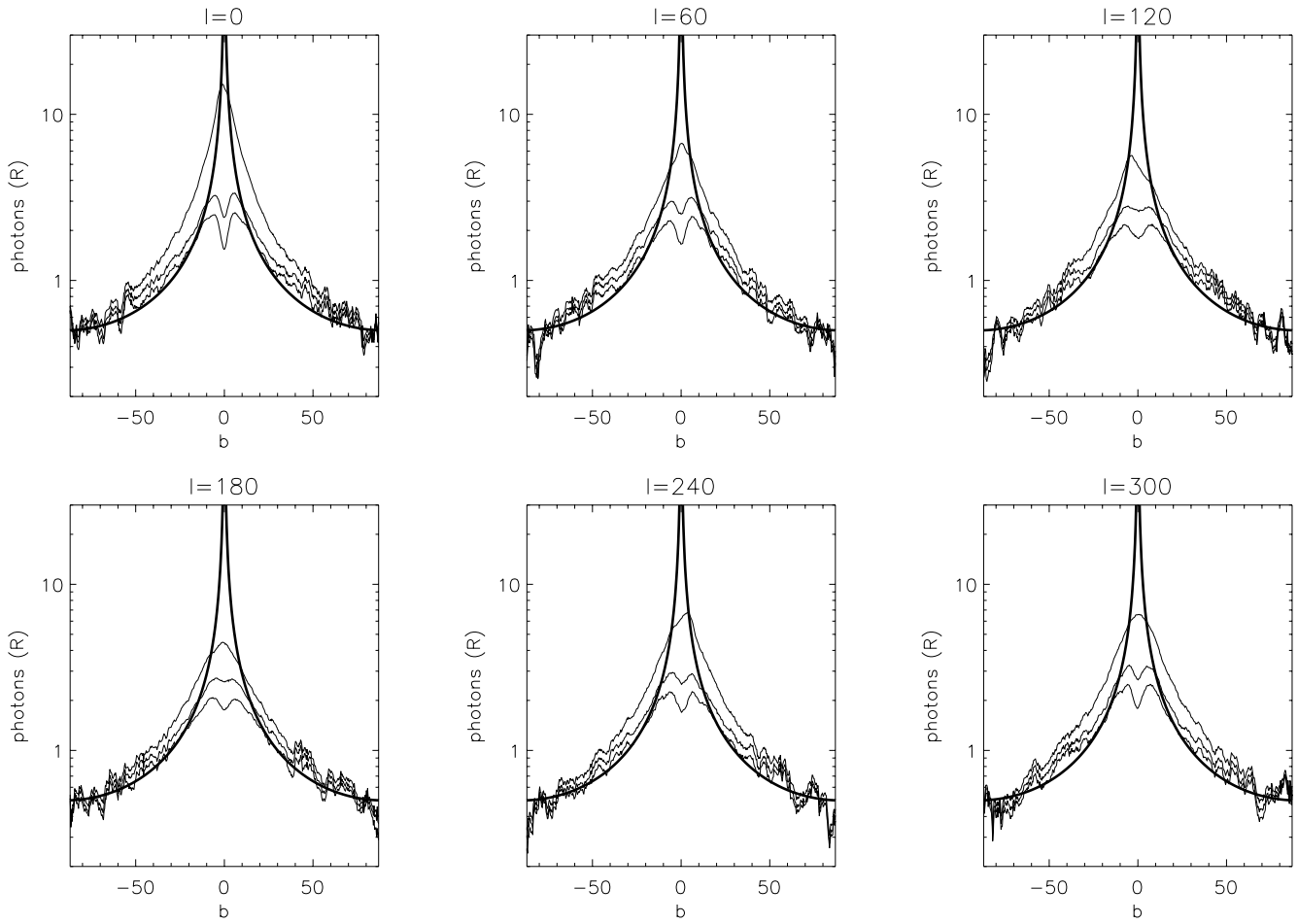

FIG. 4.—Latitudinal cuts through the simulation showing the csc $|b|$ law and three curves comprising different components of the Hα intensity: (*upper curve*) WIM emission (direct plus scattered) and the dust-scattered Hα from the point sources, (*middle curve*) WIM Hα (direct plus scattered) only, and (*lower curve*) only the direct WIM emission.

along paths in a plane-parallel layer and does not account for any scattered light component.

An important feature of our simulations is that we may determine the scattered light contribution of the Hα intensity. We find that the scattered light from midplane H II regions is typically around 10% of the total intensity at high latitudes (Fig. 3). Toward the midplane the scattered light level is larger because of the proximity of the H II regions. However, our assumption of a smooth constant density in each grid cell likely yields an overestimate of the scattered light for $b < 10°$. In reality dust will not survive in the intense radiation environment of the O stars, and more Hα photons will escape these regions without scattering than predicted by our model. Our analysis is primarily concerned with estimating the scattered light at high latitudes, and a more accurate determination of the scattered light at low latitudes requires a three-dimensional model for the ISM density, in particular in the environs of the O stars in our simulation. Reynolds (1990) estimated the scattered light contribution from Galactic H II regions to be less than 15% based on [S II]/Hα and [O III]/Hα ratios measured along sight lines toward H II regions and along sight lines in the diffuse ISM. Our model appears to confirm this estimate at high latitudes. The results of our simulation are in agreement with the Ferrara et al. (1996) model of NGC 891. In their externally viewed simulation, they estimated an Hα scattered light contribution of around 10% at 600 pc from the midplane.

We have further separated the Hα intensity according to how far from the Sun the photons originated. Figure 5 shows panels of latitudinal cuts for (*upper curve*) the total Hα intensity, and the intensity of Hα photons (direct or scattered) originating at distances greater than (*middle curve*) 3 kpc and (*lower curve*) 6 kpc from the Sun. It is clear that this simulation is dominated by photons originating within 3 kpc of the Sun. Note the absorption lane in the latitudinal cuts of photons from large distances. This arises because for sight lines above the dense dust in the H I layer the optical depth is low and we see the extended diffuse Hα from the WIM. At low latitudes the dust limits how far we can see. It should be possible to see this effect using the kinematic information provided by the WHAM survey.

The effects of dust clumping will modify our results based on a smooth density distribution. In addition to departures from the smooth scattered light cuts we have presented, Witt & Gordon (1996) showed that clumping has the overall effect of enabling photons to penetrate to larger distances than for the same dust mass arranged in a smooth geometry. The Witt & Gordon analysis considered radiation transfer in a clumpy medium surrounding a point

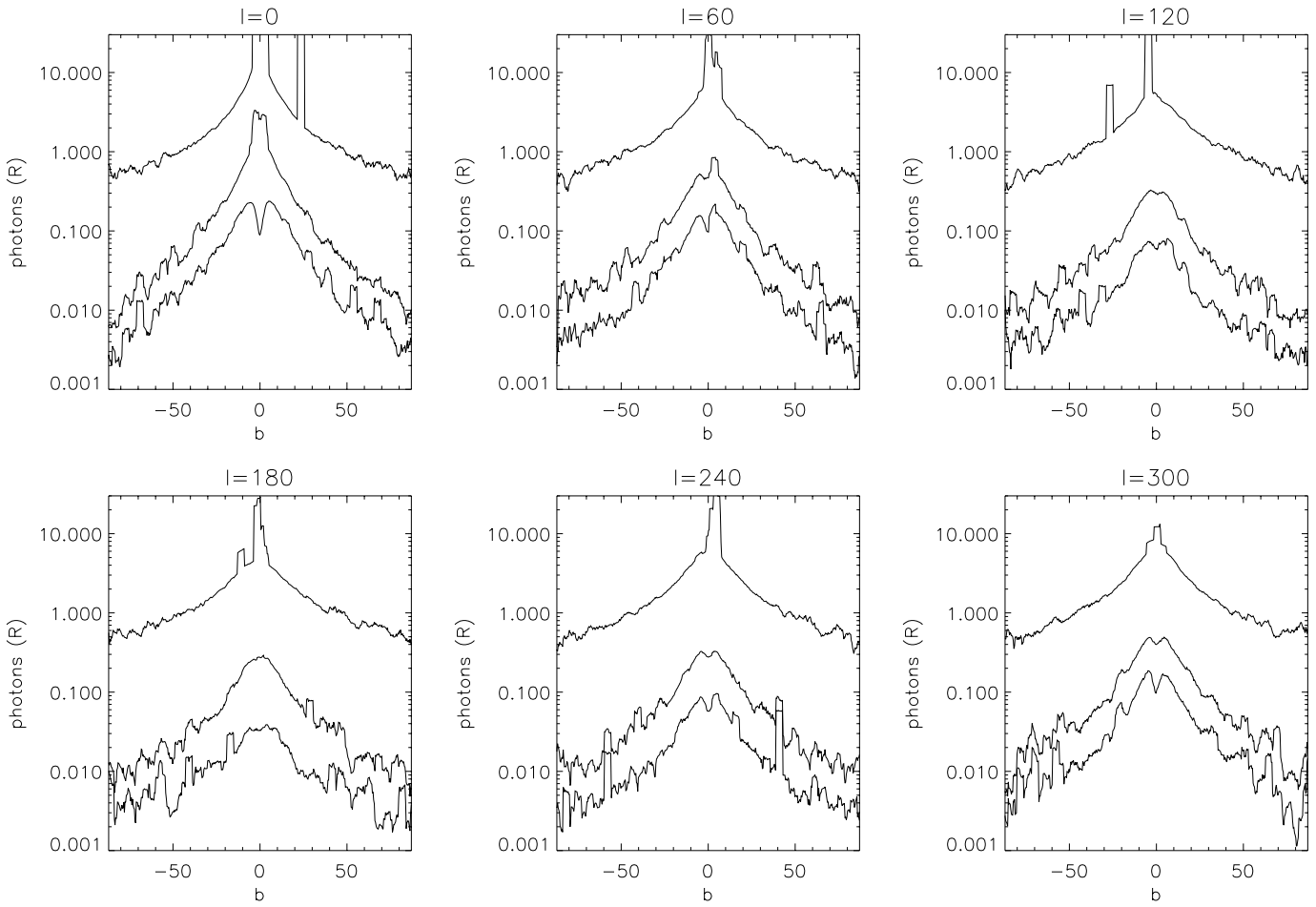

FIG. 5.—Latitudinal cuts through the simulation showing (*upper curve*) the total intensity, (*middle curve*) Hα originating from farther than 3 kpc, and (*lower curve*) farther than 6 kpc.

source, which is appropriate for the transfer of Hα photons from our point sources and will likely raise the scattered light levels. However, since the diffuse WIM emission will itself be clumpy, we intend to extend the Witt & Gordon analysis to include extended sources of emission appropriate for analysis and modeling of the WHAM data set.

4. POLARIZATION PREDICTION

With scattered light levels around 10% (as estimated from line ratio measurements and now also from our simulations), we would expect this dust-scattered Hα to be polarized. Therefore, in addition to the scattered light simulations shown above, we have also calculated the polarization arising from dust scattering. The Hα emission from the WIM and the point sources is assumed to be unpolarized, and the polarization arises from dust scattering. We have assumed that the polarization arises solely from scattering and have not considered the polarizing effect due to the transmission of radiation through regions containing aligned dust grains. Our neglect of this transmission polarization is valid for the low column density sight lines at high latitude since the transmission polarization scales with optical depth (see models by Jones 1989; Jones, Klebe, & Dickey 1992).

Figure 6 shows an all-sky map showing the predicted polarization for our simulation. The polarization is largest in the midplane regions where the amount of scattered light from the point sources is highest. The familiar centrosymmetric patterns are evident, indicative of polarization arising from scattered light from point sources, or in this simulation from concentrations of point sources. In general the polarization is perpendicular to the midplane, as expected for polarization due to scattering. Transmission polarization, which is perpendicular to the large-scale toroidal Galactic magnetic field and therefore parallel to the midplane (Mathewson & Ford 1970; Zweibel & Heiles 1997), will reduce the midplane polarization levels. The combination of low scattered light levels and polarization cancellation results in the signal-to-noise ratio of our simulations being too small to allow a detailed prediction of the polarization at high latitudes. To increase the signal-to-noise ratio, in Figure 7 we have taken 18° wide latitudinal cuts (as in the previous section) and averaged the Stokes parameters over longitude to show the average polarization as a function of latitude. The polarization is at a minimum close to the midplane, where the unpolarized direct emission dominates. The polarization then increases at latitudes just above the midplane because of the large scattered light levels. For higher latitudes, where our simulations are more accurate, the polarization decreases and is predicted to be in the range 0.1%–1%. If these predicted polarization levels could be measured, they would provide another means of

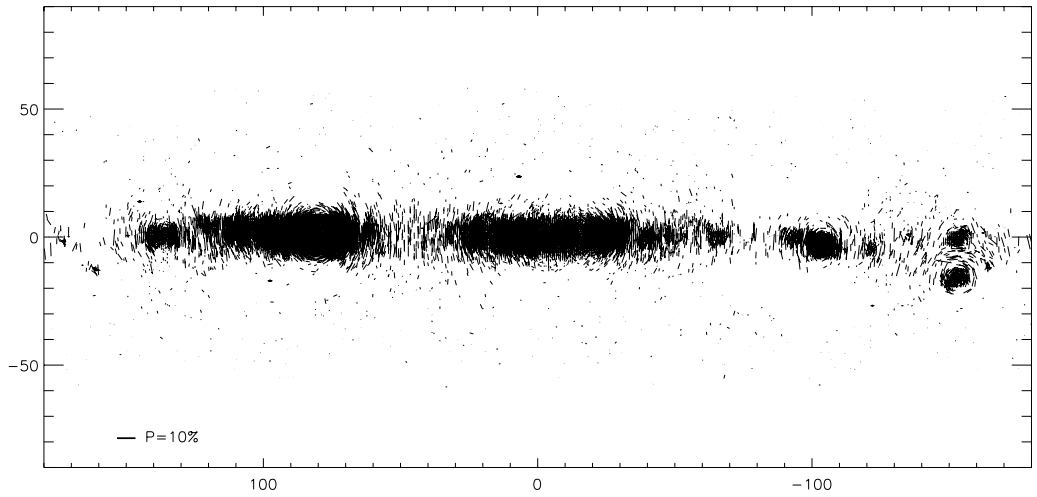

FIG. 6.—Simulated polarization map arising from dust scattering of the Hα intensity

probing the distribution of dust, the dust-to-gas ratio, and the scattering properties of the dust in the ISM.

5. SUMMARY

This paper has presented a simulation of the diffuse Hα intensity incorporating direct emission from the WIM and the dust scattering of Hα photons from the WIM and mid-plane H II regions. We have assumed that the scattering dust and WIM are distributed according to a smooth axisymmetric prescription. The H II regions are assumed to be point sources coincident with the known locations of O stars within 2.5 kpc of the Sun with Hα luminosities proportional to the ionizing flux from each source. For regions beyond 2.5 kpc, we have placed point sources randomly

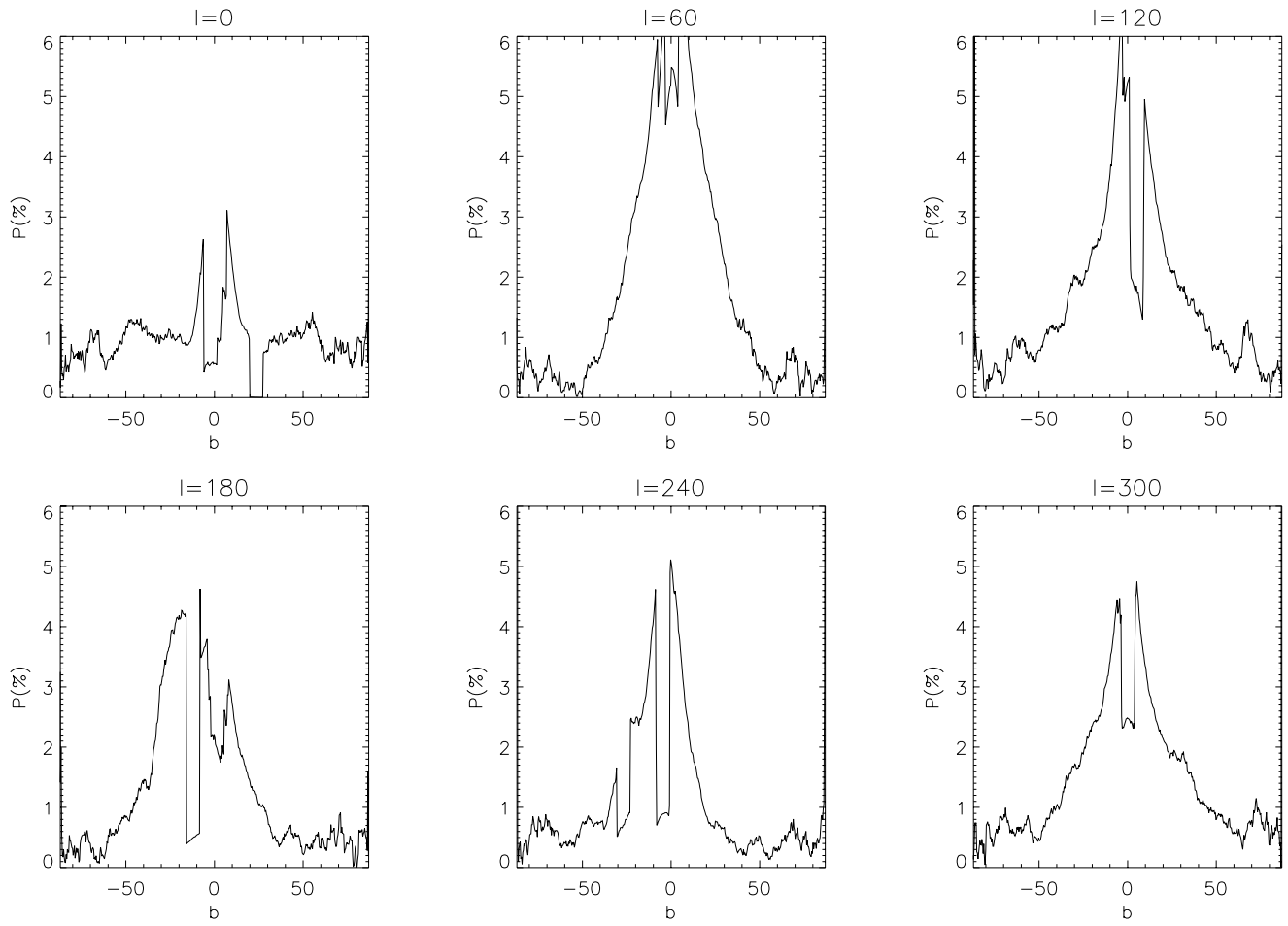

FIG. 7.— 18° wide latitudinal polarization cuts

into spiral arms and the molecular ring, such that the total Hα luminosity from H II regions is equal to that from the WIM.

Our simulation appears to reproduce the gross characteristics observed in the Hα background, namely, the csc $|b|$ law at low latitudes and departures from this at high latitudes. The departures from the csc $|b|$ law are attributed, at least in part, to a larger dust-scattered Hα component from lower latitudes. We find that dust-scattered Hα from H II regions contributes less than 20% of the total intensity, although some sight lines toward the midplane dominated by H II regions show higher scattered light levels. Our models therefore are consistent with the line ratio analysis of Reynolds (1990), who estimated the scattered light contribution to be less than 15% of the total intensity. We have also made a prediction that the scattered Hα should be polarized at around the 0.1%–1% level at high latitudes.

Preliminary results from the WHAM survey show that the Hα emission is not smooth and there are many filamentary structures present (Haffner et al. 1998; Reynolds et al. 1998). Detailed modeling of these data to determine dust-to-gas ratios, scattering phase functions, etc., will require a three-dimensional treatment of the ISM density and WIM emission, as well as inclusion of large-scale Galactic rotation to simulate line profiles for the direct and scattered line emission. Our codes are set up for this, and future modeling efforts will be directed toward developing the fully three-dimensional models demanded by the observations.

K. W. acknowledges support from NASA's Long Term Space Astrophysics Research Program (NAG 5-6039). We thank Jon Bjorkman, Barbara Whitney, and Karl Gordon for discussions relating to the forced Monte Carlo technique.

APPENDIX

RADIATION TRANSFER ALGORITHM

In our previous Monte Carlo investigations we were simulating the transfer of photons within an axisymmetric medium and formed images for external viewing. Upon exiting the simulation, scattered light images were formed by projecting the photons into (x, y) locations on image planes. Such a technique is efficient for axisymmetric, external viewing situations. However, for our current investigation where we want to form images viewed from within the density grid, we cannot use this technique since photons will rarely scatter in a direction that intersects the observer's location. We have therefore modified our algorithm as follows, so that we force weighted photons (either direct or scattered) toward the observer, thus enabling us to form all-sky images.

Hα photons are emitted either from the WIM or from the point-source H II regions. Direct photons are emitted in a direction toward the observer and have a weight

$$W_{\rm direct} = e^{-\tau}/4\pi d^2 \ , \tag{A1}$$

where τ and d are the optical depth and physical distance from the point of emission to the observer.

To calculate the scattered light contribution we first choose a random direction of travel from 4π sr and calculate the optical depth, τ_1, from the point of emission to the edge of our grid. We then force the photon to scatter at an optical depth less than τ_1, sampled from

$$\tau = -\log\,[1 - \xi(1 - e^{-\tau_1})] \ ; \tag{A2}$$

this reproduces the correct probability distribution for optical depths and ensures that all photons scatter at least once. The photons are subsequently scattered in directions that are randomly sampled from the scattering phase function (eq. [A1]). A new optical depth is then generated from $\tau = -\log \xi$ and the scattering location corresponding to this optical depth is determined. If the location is outside our grid, the photon is terminated; otherwise a new scattering angle and optical depth are generated and the photon is tracked until it exits the grid. At each scattering location we "peel off" and direct toward the observer a fraction of the photon's energy. The weight of this "peeled off" photon is

$$W_{\rm scatt} = a^N(1 - e^{-\tau_1})e^{-\tau_2}{\rm HG}(\theta)/d_2^2 \ , \tag{A3}$$

where N is the number of scatterings the photon has undergone up to that point, τ_1 is the first optical depth, and τ_2 and d_2 are the optical depth and physical distance from the scattering location to the observer. The function ${\rm HG}(\theta)$ weights the photon by the scattering phase function, where θ is the angle through which we force the photon to scatter toward the observer. The total intensity is the sum of the weights of the direct (eq. [A2]) and scattered (eq. [A3]) photons. We have tested this algorithm for external viewing situations against several "regular" Monte Carlo codes that do not employ any forced scattering or weighting algorithms and find it to be accurate and efficient.

REFERENCES

Bianchi, S., Ferrara, A., & Giovanardi, C. 1996, ApJ, 465, 127
Bland-Hawthorn, J., & Maloney, P. R. 1999, ApJ, 510, L33
Calzetti, D., Bohlin, R. C., Gordon, K. D., Witt, A. N., & Bianchi, L. 1995, ApJ, 446, L97
Cox, D. P., & Reynolds, R. J. 1987, ARA&A, 25, 303
Dickey, J. M., & Lockman, F. J. 1990, ARA&A, 28, 215
Domgörgen, H., & Mathis, J. S. 1994, ApJ, 428, 647
Dove, J. B., & Shull, J. M. 1994, ApJ, 430, 222
Dove, J. B., Shull, J. M., & Ferrara, A. 1999, ApJ, in press
Elmegreen, B. G. 1997, ApJ, 477, 196
———. 1998, Publ. Astron. Soc. Australia, 15, 74
Ferguson, A. M. N., Wyse, R. F. G., & Gallagher, J. S. 1996, AJ, 111, 2265
Ferrara, A., Bianchi, S., Dettmar, R., & Giovanardi, C. 1996, ApJ, 467, L72
Ferrière, K. 1998, ApJ, 503, 700
Garmany, C. D., Conti, P. S., & Chiosi, C. 1982, ApJ, 263, 777
Gordon, K. D., Witt, A. N., Carruthers, G. R., Christensen, S. A., & Dohne, B. C. 1994, ApJ, 432, 641
Haffner, L. M., Reynolds, R. J., & Tufte, S. L. 1998, ApJ, 501, L83
Hurwitz, M. 1994, ApJ, 433, 149
Jones, T. J. 1989, ApJ, 346, 728
Jones, T. J., Klebe, D., & Dickey, J. 1992, ApJ, 389, 602
Martin, P. G. 1988, ApJS, 66, 125

Mathewson, D. S., & Ford, V. L. 1970, MmRAS, 74, 139
Mathis, J. S., Rumpl, W., & Nordsieck, K. H. 1977, ApJ, 217, 425
Miller, W. W., & Cox, D. P. 1993, ApJ, 417, 579
Murthy, J., & Henry, R. C. 1995, ApJ, 448, 848
Reynolds, R. J. 1988, ApJ, 333, 341
———. 1990, in IAU Symp. 139, The Galactic and Extragalactic Background Radiation, ed. S. Boyer & C. Leinert (Dordrecht: Kluwer), 157
Reynolds, R. J., Tufte, S. L., Haffner, L. M., Jaehnig, K., & Percival, J. W. 1998, Publ. Astron. Soc. Australia, 15, 14
Reynolds, R. J., Tufte, S. L., Kung, D. T., McCullough, P. R., & Heiles, C. R. 1995, ApJ, 448, 715
Sciama, D. W. 1995, ApJ, 448, 667
Snowden, S. 1986, Ph.D. thesis, Univ. Wisconsin–Madison
Taylor, J. H., & Cordes, J. M. 1993, ApJ, 411, 674
Veilleux, S., Cecile, G., & Bland-Hawthorn, J. 1995, ApJ, 445, 152
Walterbos, R. A. M., & Braun, R. 1994, ApJ, 431, 156
White, R. L. 1979, ApJ, 229, 954
Whitney, B. A., Kenyon, S. J., & Gomez, M. 1997, ApJ, 485, 703
Witt, A. N., & Gordon, K. G. 1996, ApJ, 463, 681
Wood, K. 1997, ApJ, 477, L25
Wood, K., & Jones, T. J. 1997, AJ, 114, 1405
Zweibel, E. G., & Heiles, C. 1997, Nature, 385, 131